Biomechanical Implications of Spinopelvic Alignment on Femoral Head Cartilage and the Proximal Femoral Physis in Slipped Capital Femoral Epiphysis: A Theoretical Finite Element Analysis

Yogesh Kumaran MS[1,2], Muzammil Mumtaz PhD[1], Carmen Quatman MD, PhD[2], Julie Balch-Samora MD, PhD[3], Sophia Soehnlen MS[1,2], Brett Hoffman BS[1], Sudharshan Tripathi MS[1], Norihiro Nishida MD, PhD[4], Vijay K. Goel PhD[1]

[1]Engineering Center for Orthopedic Research (E-CORE), Departments of Bioengineering and Orthopaedic Surgery, University of Toledo, Toledo, OH, USA

[2]Ohio State University Wexner Medical Center, Department and Orthopaedics, Columbus, OH, USA

[3]Nationwide Children's Hospital, Department of Orthopedics, Columbus, OH, USA

[4]Yamaguchi University Hospital, Department of Orthopaedic Surgery, Ube, Yamaguchi, Japan

Address Correspondence to:
Vijay K. Goel, PhD
Distinguished University Professor
Endowed Chair & McMaster-Gardner Professor of Orthopaedic Bioengineering
Co-Director, Engineering Center for Orthopaedic Research Excellence (E-CORE)
Departments of Bioengineering and Orthopaedic Surgery
Colleges of Engineering and Medicine

University of Toledo, Toledo, OH, USA, 43606
Mail to: Univ of Toledo, 2801 West Bancroft Street, MS 303, NI Hall, Room 5046, Toledo, OH 43606
Ph: 419-530-8035; FAX: 419-530-8076; Vijay.Goel@utoledo.edu
The work was supported in part by the NSF Industry/University Cooperative Research Center at the University of California at San Francisco, CA, the Ohio State University, Columbus, Ohio, and the University of Toledo, Toledo, OH (www.nsfcdmi.org).

Abstract

Background

Slipped capital femoral epiphysis (SCFE) is a prevalent pediatric hip disorder. Recent studies suggest the spine's sagittal profile may influence the proximal femoral growth plate's slippage, an aspect not extensively explored. This study utilizes finite element analysis to investigate how different spinopelvic alignments affect shear stress and potential slippage at the growth plate.

Methods

A finite element model was developed from CT scans of a healthy adult male lumbar spine, pelvis, and femurs. The model was subjected to various sagittal alignments through rotational boundary conditions. Simulations of two-leg stance, one-leg stance, walking heel strike, ascending stairs heel strike, and descending stairs heel strike were conducted. Parameters measured included hip joint contact area, stress, and maximum Tresca (shear) stress on the growth plate.

Findings

Posterior pelvic tilt cases indicated larger shear stresses compared to the anterior pelvic tilt variants except in two leg stance. Two leg stance resulted in decreases in the posterior

tilted pelvi variants compared to anterior tilted pelvi, however a combination of posterior pelvic tilt and high pelvic incidence indicated larger shear stresses on the growth plate. One leg stance and heal strike resulted in higher shear stress on the growth plate in posterior pelvic tilt variants compared to anterior pelvic tilt, with a combination of posterior pelvic tilt and high pelvic incidence resulting in the largest shear stress.

Interpretation

Our findings suggest that posterior pelvic tilt and high pelvic incidence can lead to increased shear stress at the growth plate. Activities performed in patients with these alignments may predispose to biomechanical loading that shears the growth plate, potentially causing slippage.

Keywords: Slipped capital femoral epiphysis, spinopelvic parameters, finite element analysis

Introduction

Slipped capital femoral epiphysis (SCFE) is a multifactorial pathology of the hip commonly affecting children between the ages of 8 and 15 years with an incidence of 0.3-2/100,000 [1]. Early identification of high-risk patients for SCFE is crucial for implementing preventive strategies against slippage at the proximal femoral physis and its adverse sequelae [2]. Obesity, endocrinopathies, and vitamin D deficiency are risk factors that have been implicated in its development [3, 4]. Biomechanical factors, including acetabular version, repetitive weight-bearing activities, sports, and other physical exertions, also contribute to increased shear stresses at the proximal femoral physis, leading to slippage [5, 6]. Recent studies have also pointed to the sagittal profile of the spinopelvic complex as a contributing factor to growth plate shear and slippage [7, 8].

Sagittal balance refers to the physiologic alignment of the spine which maximizes kinetic efficiency and minimizes mechanical stress. Balance exists when an individual's weight is positioned on a vertical axis aligned slightly posterior to the rotational axis of the femoral heads [9, 10]. Spinopelvic parameters determine the overall sagittal balance of the spinopelvic complex and include lumbar lordosis (LL), sacral slope (SS), pelvic tilt

(PT), and pelvic incidence (PI) (Figure 1) [11-14].

While the relationship between hip and spine mechanics has been extensively studied in adults, its impact on the SCFE population remains less explored [15, 16]. Controversy exists on whether PI and other spinopelvic parameters contribute to SCFE. A cadaveric study performed by Gebhart et al identified smaller PI angles in post-SCFE deformity patients compared to normal specimens [7]. On the other hand, a retrospective study performed by Wako et al determined no relationship between PI and SCFE [8]. These discrepancies highlight the need for biomechanical analyses to understand the role of load distribution on the femoro-acetabular joint and proximal femoral physis due to variations in sagittal spinopelvic parameters.

To the best of the authors' knowledge, this is the first biomechanical study to examine SCFE encompassing the complete spinopelvic complex, including the femur, hip joint, pelvis, and spine [17-21]. We hypothesize that sagittal spinopelvic alignment influences stress redistribution on the femoral head and proximal femoral physis. This study utilizes a theoretical finite element (FE) model to investigate the contribution of sagittal spinopelvic parameters to SCFE biomechanics.

Methods

Original FE model creation

A non-linear, ligamentous FE model was developed using computed tomographic (CT) scans of a healthy adult lumbar spine, pelvis, and femur with no abnormalities, deformities, or severe degeneration. The CT scans were reconstructed and segmented using MIMICS software (Materialize Inc., Leuven, Belgium). Mesh was applied to the reconstructed geometry using Meshlab Open-Source Software [22].

Abaqus 2019 (Dassault Systèmes, Simulia Inc., Providence, RI, USA) was used to assemble the meshed components and perform the subsequent analyses. All geometries were imported and the "tri to tet" feature was used to convert the triangular shell surface mesh into solid tetrahedral mesh (C3D4). The vertebral bodies, pelvis and femurs were modelled with a 0.5-1mm cortical bone shell containing a core of cancellous bone. The annulus fibrosa was simulated as a composite solid containing alternating ±30º collagen fibers modelled as rebar elements using the "no compression" property. The nucleus pulposa was simulated as a linear elastic material. The facet joints were modeled using three-dimensional gap elements with a defined clearance of 0.5mm. The ligamentous structures of the spine and sacroiliac joints were modelled as truss elements. Table 1 lists

the material properties used in the FE models [23-26]. Validation of the vertebral components of the lumbar spine are described elsewhere [25-30].

Hip joint creation and validation

The femoral heads were positioned relative to the pelvis according to anatomical parameters described by Wu et al [31]. Femoral head and acetabular cartilage were modelled by adding a 1mm layer of mesh with hybrid formulation (C3D4H) applied on both surfaces [32]. Ten to twelve random nodal coordinates of the femoral heads and acetebulae were obtained to create a best fit sphere whose centroid coordinates were used to properly place the femoral heads within the acetabulae [33]. The cartilage was modelled with incompressible, neo-Hookean hyperelastic material properties [34]. The hip joint was adjusted until the joint space fell within reported parameters determined by Goker et al (3.43± 0.40 for the right hip and 3.48±0.68 for the left hip) [35]. The hip joint capsule was created in Solidworks 2022 (Dassault Systèmes, Simulia Inc., Providence, RI, USA) based on circumferential locations defined by Stewart et al [36]. Hyperelastic material properties were applied to this geometry based on the Ogden strain energy potential and utilizing uniaxial test data based on a study performed by Stewart et al [36]. Muscles spanning the hip joint from their physiologic origins and insertions were

included in the FE model as connector elements with stiffnesses based on Phillips et al (Table 1) [37].

To assess and validate proper functionality of the hip joints, contact stresses and areas were evaluated based on simulated positions corresponding to two-leg stance (2LS), walking heel strike (WHS), ascending stairs heel strike (AHS), and descending stairs heel strike (DHS) per femur angles based on Bergmann et al's data [38, 39]. Peak and average contact stresses (MPa) and contact area (mm^2) at the hip joint were validated against previous studies [34, 39, 40].

The growth plate was modelled by sectioning 7mm of the femoral head [41]. The right and left femur physeal-diaphysis angle (PDA) was 39º and 44º, respectively (Figure 2) [20]. Elastic material properties were applied to the growth plate (Table 1) [17, 20, 21, 42]. The original model had the following spinopelvic parameters: SS=31.7º, PT=9.8º, PI=41.5º, and LL=46º.

This model was modified with various SS and PT angles by rotating the sacrum and pelvis, respectively [43]. The SS angles were incrementally increased by 5º to obtain PIs of 36º, 41º, 46º, and 51º, respectively. To understand the influence of PT on the growth plate, each SS modified model had two variants: high PT (posteriorly tilted) and low PT

(anteriorly tilted) cases (Table 2).

Loads, boundary conditions, and analysis

A 400 N compressive follower load was applied following the curvature of the L1-L5 vertebrae through wire elements to simulate the passive effect of muscle forces and weight of the upper trunk [39]. A 500 N force was distributed between the sacral promontory and pubic symphisys to simulate body weight on the pelvis and femur [39]. Two leg stance (2LS), right leg one leg stance (1LS), AHS, DHS, and WHS cases were simulated to evaluate various activities' impact on the femoral heads and growth plate. Boundary conditions were applied at the base of the femurs to fix the model. Average contact stress and contact area of the femoral head was calculated for each motion and alignment. To evaluate shear stresses on the proximal femoral growth plate, maximum Tresca stresses were recorded.

Results

Validation was performed on the model to confirm functionality of the hip joints. Average contact stresses were found to be in range of previous studies with peak contact stresses being slightly higher (Tables 3, 5 and 6). Regarding contact areas, values were in-line of previous studies (Tables 4 and 7).

Overall, higher PT indicated larger contact areas compared to low PT variants. A combination of higher PT and PI resulted in substantially larger contact areas compared to low PT and low PI for each simulated motion (~18% increases) (Figure 3).

Regarding hip contact stresses, the heel strike simulations (WHS, AHS, and DHS) resulted in the largest values compared to 2LS and 1LS, especially in the PI41 cases. The 1LS and 2LS simulations indicated that as PT increased, larger contact stresses were mitigated (Figure 4). All heel strike simulations showed a similar trend with higher contact stresses in the high PT variants (~10% increases), except for WHS. In WHS, PI41-High PT resulted in the largest contact stress with marginal changes in higher PIs. AHS indicated lower contact stresses in PI52 compared to all other cases in AHS, with PI46 indicating the largest contact stress. In DHS, PI41 indicated the largest contact stresses compared to the other cases.

Regarding Tresca stresses, heel strike simulations resulted in the largest stresses on the growth plate with AHS indicating the largest values overall. High PT variants resulted in larger shear stresses compared to the low PT variants (~18% increases) except in 2LS. A combination of high PT and PI resulted in the largest overall Tresca stress on the growth plate for each simulated case (10-24% increases) (Figure 6). In 1LS, WHS, AHS and

DHS, Tresca stresses for the high PT variant of PI36 was comparable to PI46-High PT, though smaller than PI52-High PT.

Discussion

The aim of the current study was to elucidate the role of spinopelvic parameters on the hip joint and an open femoral growth plate to assess the potential for development of SCFE. Current research in this area is limited, with only a few studies leveraging FE models to examine SCFE under different loading scenarios [17-21, 42]. Our findings revealed that a combination of posterior pelvic tilt (PT) and high pelvic incidence (PI) angles lead to large hip contact area and elevated shear stresses on the proximal femoral physis.

Previous reports have stated that higher pelvic incidence and sacral slope angles contribute to larger mechanical stresses on the hip joint [43, 44]. Lazennec and colleagues described clinical consequences of sagittal imbalance in pelvic and sub-pelvic regions in patients and eluded to how atypical postures and morphology contribute to disturbances in the hip joint [15, 16]. Disruption of the spinopelvic complex displaces mechanical forces and increases load absorption on the intervertebral discs and femoroacetabular joints. The present study suggests that various spinopelvic alignments distribute stresses

at the hip joint and growth plate differently, specifically patients with high pelvic incidence and posterior pelvic tilt potentially being more prone to slippage in SCFE [6]. Conflicting results are present in the current literature regarding PI and SCFE. An osteological, adult cadaveric study performed by Gebhart et al identified lower PI in post-SCFE specimens compared to a control of normal specimens [7] [45, 46]. Our results indicate that lower pelvic incidence angles contribute to larger contact stress at the hip joint, and seldom to shear stresses on the epiphyseal growth plate, which are two components that are risk factors for SCFE [6]. Additionally, the type of activity performed and degree of pelvic tilt also determine the overall shear at the growth plate. For instance, some postures indicated that low pelvic incidence combined with posterior pelvic tilt (PI36-HighPT) contributed to shear at the growth plate more than higher pelvic incidence (PI46). However, in most postures, high pelvic incidence alone and posterior pelvic tilt combined with high pelvic incidence resulted in the largest shear at the growth plate. This finding can be attributed to the high sacral slope and lumbar lordosis angles distributing a shear load through the femur and proximal femoral growth plate. Contrast this to the low pelvic incidence cases where the model remains more vertical due to a low sacral slope, the load distributing from the lumbar spine through the femoro-acetabular joint and

growth plate were likely compressive forces rather than shear.

A retrospective observational study by Wako et al did not identify a relationship between PI and SCFE, though determined a significance in retroverted acetabuli and excessive coverage of the anterior and superior acetabulum in SCFE patients compared to a control group [8]. Current studies have mixed results on whether SCFE-affected hips are associated with the phenomena of anteversion or retroversion [7, 8, 47, 48]. Additionally, many studies do not correct for pelvic tilt which has the potential to overestimate acetabular version [49, 50]. In the current study, two pelvic tilt variants were examined for posterior and anterior pelvic tilt. Results indicated high contact area in the posterior pelvic tilt variants compared to anterior tilt which can be attributed to larger coverage of the posterior femoral head with the superior acetabulum. Contact stresses resulted in the same trend in 2LS and 1LS, though the opposite was seen in walking, ascending stairs, and descending stairs as posterior tilted variants indicated higher contact stress. Since stress is defined as the force applied over a certain area, this may seen counterintuitive, though as described by Henak et al, contact location, distribution and direction change during walking, ascending stairs, and descending stairs. In our case, the anterior tilted pelvi along with the angles of the femur in the heel strike simulations distributed the load

anteriorly and superiorly compared to posterior tilt, thus agreeing with Henak and colleagues' findings [51]. Our results suggest that patients may experience higher contact stress on the femoral head cartilage during gait, especially in patients with excess posterior pelvic tilt [8, 49, 51-53]. Along with higher femoral head contact stress, patients with posterior pelvic tilt may be more prone to slip due to higher shear stresses at the growth plate.

In the adult population, atypical pelvic postures produce consequences to the stability of the hip after arthroplasty, contributing further to imbalance of sagittal spinopelvic parameters [15, 16]. Furthermore, high pelvic incidence has been suggested to contribute to excessive loading on the femoral head cartilage leading to osteoarthritis of the hip [44, 54, 55]. Regarding SCFE, osteoarthritis has remained a problematic sequealae in young adult patients who experienced severe slip or surgical pinning to repair the proximal femoral physis [56, 57]. Long term follow-up of these patients commonly exhibit hip cartilage degeneration due to CAM deformity and femoroacetbular impingement [58, 59]. Based on these previous findings and the current study's results, a pediatric patients dynamic mechanical history, surgical history of pinning, and sagittal alignment may suggest a compounding deleterious effect on the hip cartilage and early-onset

osteoarthritis in sagittally imbalanced patients [60]. Future clinical and biomechanical studies will further explore this topic.

The current study's finite element (FE) model, while insightful, is subject to certain limitations. Notably, we employed an adult model in this theoretical analysis. This decision stemmed from the fact that CT imaging for SCFE patients often focuses solely on the pelvic area, excluding critical details like lumbar lordosis and sacral slope. Conducting additional spine-focused CT scans would unnecessarily expose children to extra radiation. Consequently, crafting patient-specific models encompassing the complete spinopelvic complex with varied spinal alignments in pediatric SCFE patients necessitated certain simplifications. While it's recognized that pelvic and spinal morphology evolve from childhood through adulthood, the study's results are deemed reliable and indicate a potential mechanical linkage between spinopelvic parameters and the pediatric growth plate. The absence of validated pediatric spine models in the literature, predominantly due to the lack of pediatric cadaver studies, and the prevalent reliance on scaling methods for spine modeling in children, further justified our approach Furthermore, while the reference range for pelvic incidence (PI) in adults spans from 33 to 85, our study faced a technical limitation in that our finite element (FE) model could

only simulate PIs between 36 and 51 [61]. This restriction was due to element penetration and contact errors encountered when attempting to adjust the PI beyond 51. As a result, the range of PIs explored in our study was narrower than ideal. This constraint potentially limits the generalizability of our findings across the full spectrum of PI values typically observed in clinical settings. Additionally, muscle forces spanning the hip and spine were simplified as passive connector elements with elastic properties and follower loads. Global mechanics were of interest to the authors rather than micro-mechanics, therefore the growth plate was simulated as a linear, elastic material property [17, 21, 42]. Additionally, the physeal-disphyseal angle and physeal thickness were held constant due to variation of plate thickness and angle having little contribution to stresses on the growth plate [17, 18, 20]. Lastly, only a male model was constructed in this study. The biomechanics of female pelvi may distribute loads differently compared to male pelvi, therefore future studies should examine sexual dimorphism in pediatric pelvi.

This study suggests that patients with specific sagittal alignments such as low pelvic incidences in some activities and high pelvic incidences combined with posterior tilted pelvi may be more prone to slip due to changes in contact stresses at the femoral head and high shear stress on the proximal femoral growth plate. It may be necessary for hip

preservation surgeons to consider sagittal imbalance as a potential risk factor for SCFE, though future studies are required to confirm this theory.

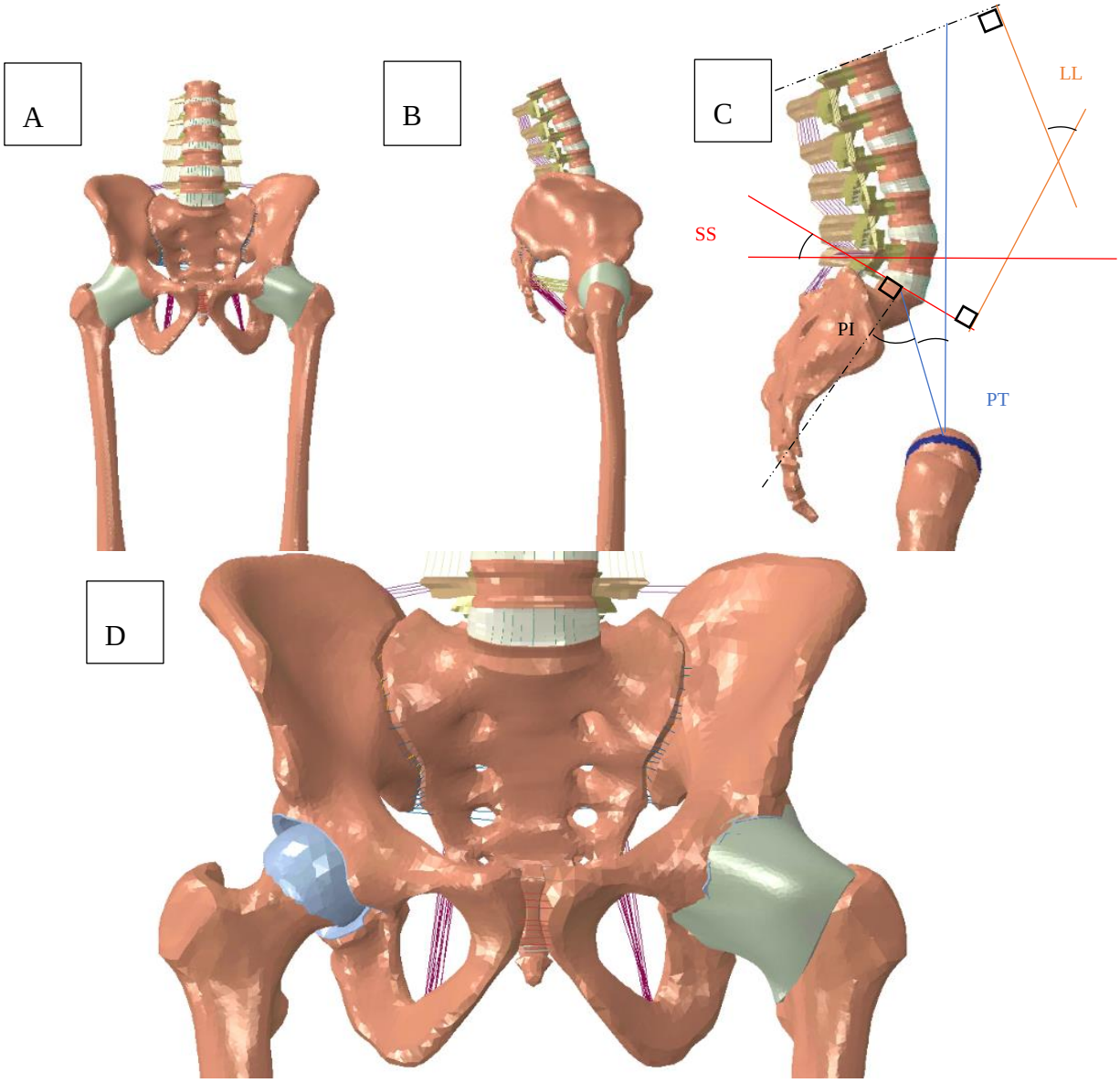

Figure 1: Finite element model with the following spinopelvic parameters: PI = 46, SS = 26.7, PT = 20, LL = 51. A) Represents the anterior view of the model, B) represents the sagittal profile, C) represents the spinopelvic angles (PT, PI, SS, LL), D) represents the

articulating surface of the hip joint with the capsule removed (right hip) and the capsule surrounding the hip joint (left hip).

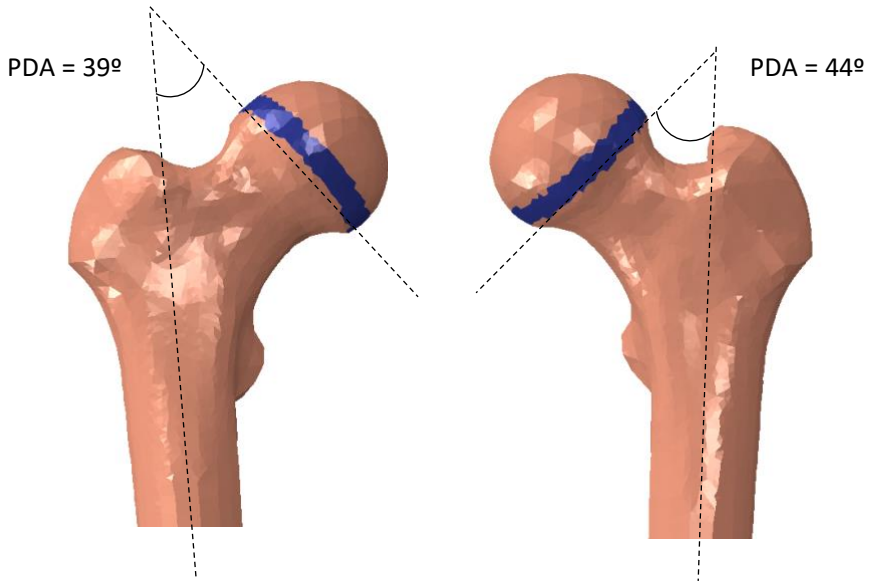

Figure 2: Representation of the right and left femurs with 7mm thick growth plates. The PDA for the right and left femurs were 39º and 44º, respectively. The PDA was measured by drawing a line through the intremedullary canal in the femur and an intersecting line parallel to the base of the epiphyseal growth plate.

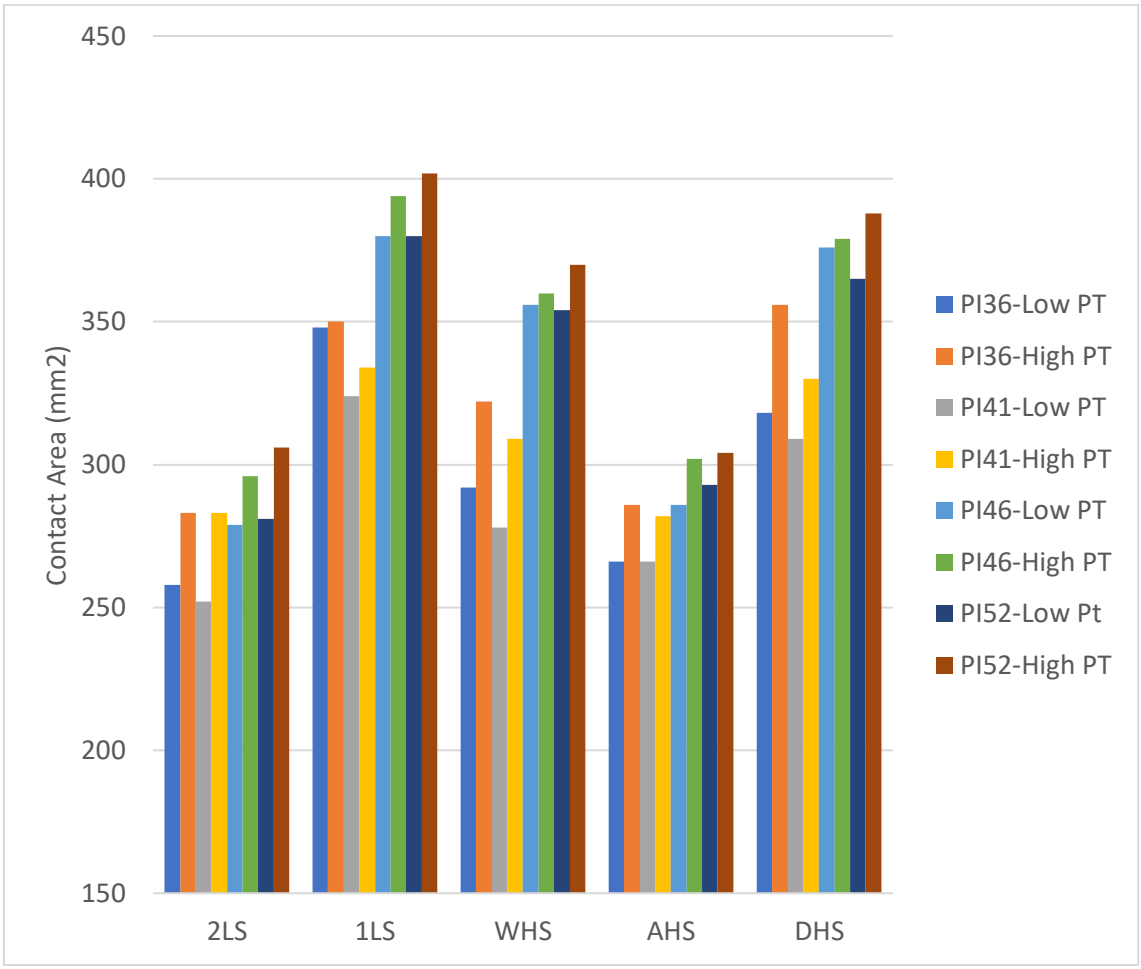

Figure 3: Contact area (mm^2) on the femoral head cartilage in various stances. 2LS refers to two leg stance, 1LS refers to one leg stance, WHS refers to walking heel-strike, AHS refers to ascending stairs heel strike, and DHS refers to descending stairs heel strike.

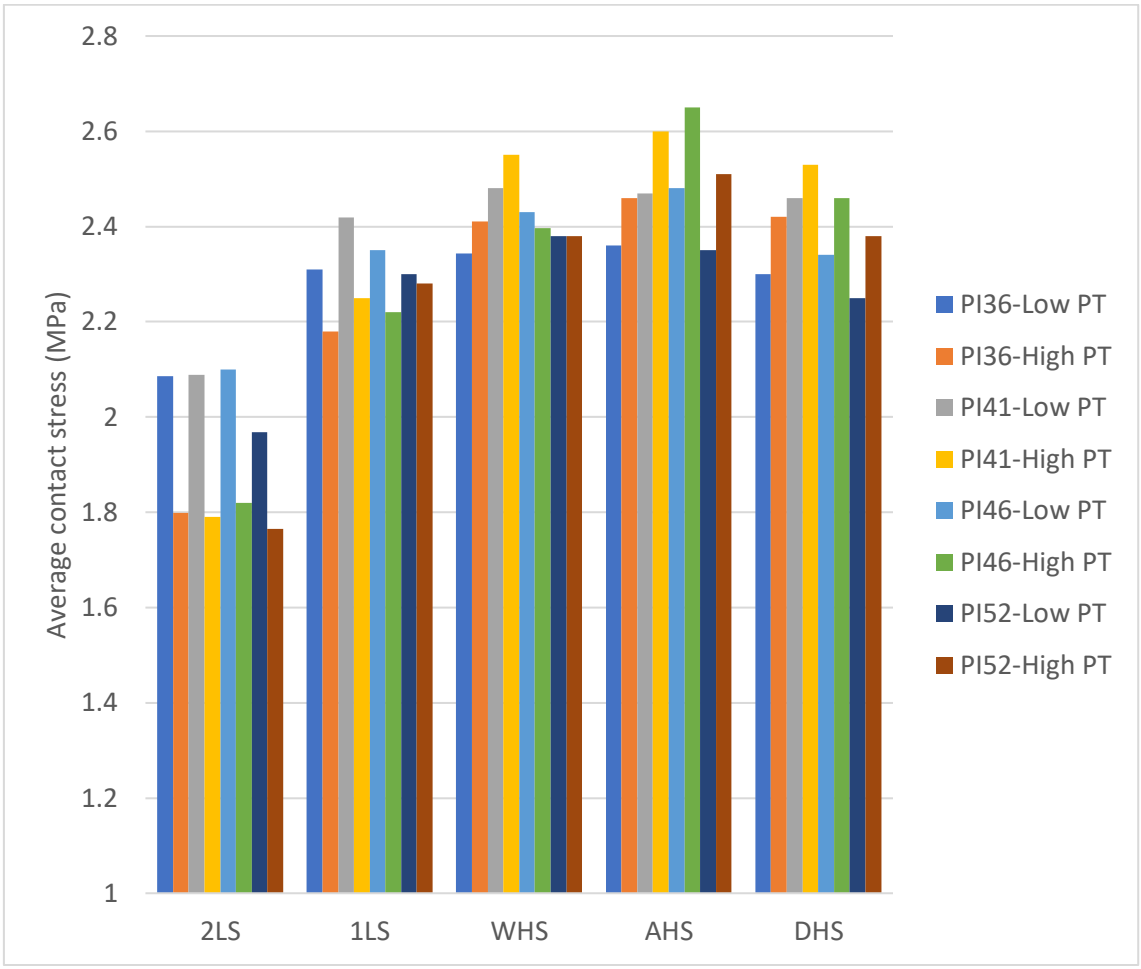

Figure 4: Average hip contact stress (MPa) on the femoral head cartilage in various stances.

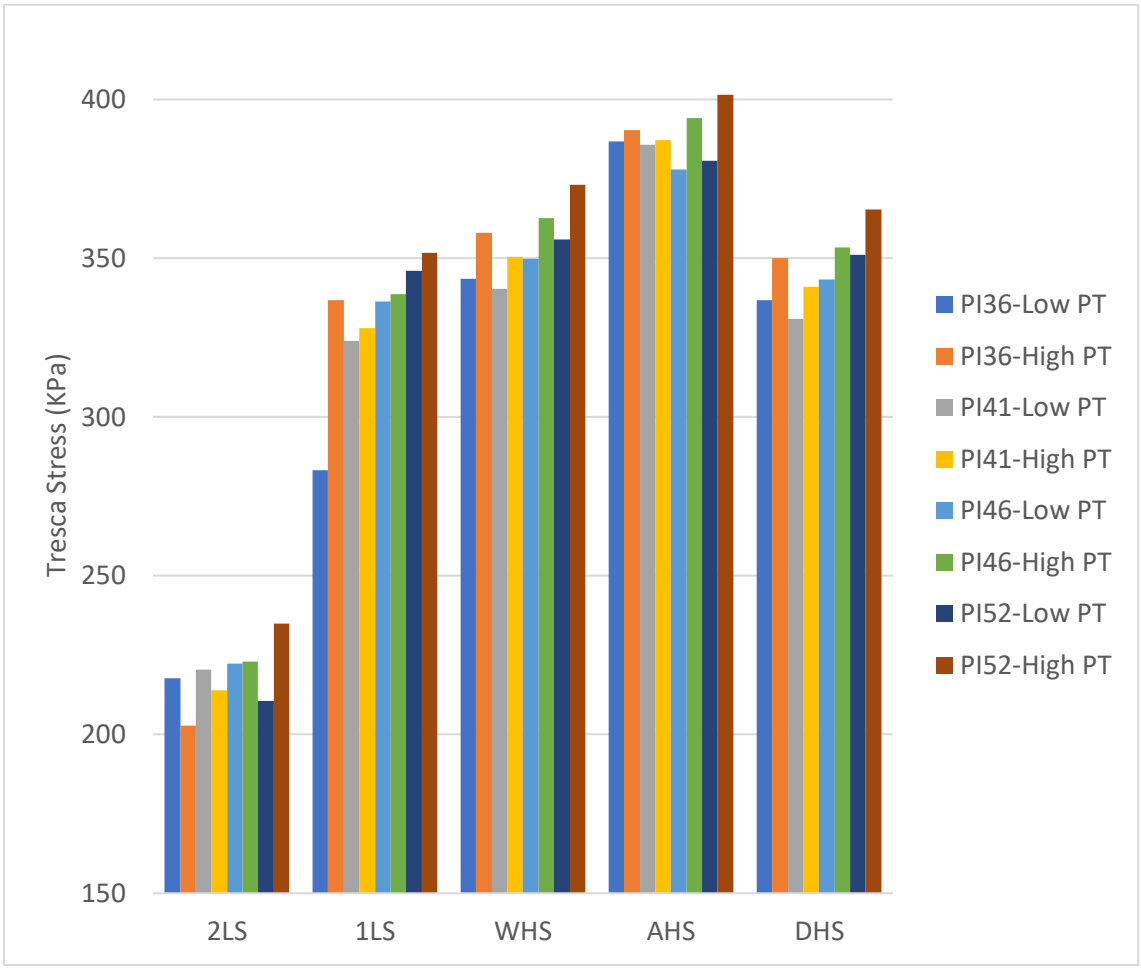

Figure 5: Maximum Tresca (shear) stress in KPa on the growth plate in various stances.

1 Table 1: Material properties assigned to the finite element models [17, 21, 27, 34, 36,

2 37, 39, 51, 62-65]. E represents Young's modulus, v represents Poisson's ratio.

Component	Material Properties	Constitute Relation	Element Type
Vertebral Cortical Bone	E= 12000MPa	Isotropic, Elastic	8 Node Brick Element (C3D8)
	v= 0.3		
Vertebral Cancellous Bone	E= 100MPa	Isotropic, Elastic	4 Node Tetrahedral Element (C3D4)
	v= 0.2		
Pelvis Cortical Bone (Sacrum, Ilium)	E= 17000MPa	Isotropic, Elastic	4 Node Tetrahedral Element (C3D4)
	v= 0.3		
Sacrum Cancellous Bone	Heterogenous	Isotropic, Elastic	4 Node Tetrahedral Element (C3D4)
Ilium Cancellous Bone	E= 70 MPa	Isotropic, Elastic	
	v= 0.2		4 Node Tetrahedral Element (C3D4)
Femur Cortical Bone	E= 17000MPa	Isotropic, Elastic	4 Node Tetrahedral Element (C3D4)
	v= 0.29		
Femur Cancellous Bone	E= 100 MPa	Isotropic, Elastic	4 Node Tetrahedral Element (C3D4)
	v= 0.2		
Ground Substance of Annulus Fibrosis	c10= 0.035		
	k1= 0.296	Anisotropic, Hyperelastic (HGO)	8 Node Brick Element (C3D8)
	k2= 65		
Nucleus Pulposus	E= 1 MPa	Isotropic, Elastic	8 Node Brick Element (C3D8)
	v= 0.499		

Hip Cartilage	C10 = 6.8 D1= 0.001	Neo-Hookean, Hyperelastic	4 Node Tetrahedral, Hybrid Element (C3D4H)
Hip Capsule	Uniaxial Test Data	Ogden, Hyperelastic	4 Node Tetrahedral, Hybrid Element (C3D4H)
Growth Plate	E=5 MPa	Isotropic, Elastic	4 Node Tetrahedral Element (C3D4)
	v=0.49		
Anterior Longitudinal	7.8 MPa (<12%), 20 MPa (>12%)	Non-linear, Hypoelastic	Truss Element (T3D2)
Posterior Longitudinal	10 MPa (<11%), 20 MPa (>11%)	Non-linear, Hypoelastic	Truss Element (T3D2)
Ligamentum Flavum	15 MPa (<6.2%), 19.5 MPa (>6.2%)	Non-linear, Hypoelastic	Truss Element (T3D2)
Intertransverse	10 MPa (<18%), 58.7 MPa (>18%)	Non-linear, Hypoelastic	Truss Element (T3D2)
Interspinous	10 MPa (<14%), 11.6 MPa (>14%)	Non-linear, Hypoelastic	Truss Element (T3D2)
Supraspinous	8 MPa (<20%), 15 MPa (>20%)	Non-linear, Hypoelastic	Truss Element (T3D2)

Capsular	7.5 MPa (<25%), 32.9 MPa (>25%)	Non-linear, Hypoelastic	Truss Element (T3D2)
Anterior SIJ	125 MPa (5%), 325 MPa (>10%), 316 MPa (>15%)	Non-linear, Hypoelastic	Truss Element (T3D2)
Short Posterior SI	43 MPa (5%), 113 MPa (>10%), 110 MPa (>15%)	Non-linear, Hypoelastic	Truss Element (T3D2)
Long Posterior SI	150 MPa (5%), 391 MPa (>10%), 381 MPa (>15%)	Non-linear, Hypoelastic	Truss Element (T3D2)
Interosseous	40 MPa (5%), 105 MPa (>10%), 102 MPa (>15%)	Non-linear, Hypoelastic	Truss Element (T3D2)
Sacrospinous	304 MPa (5%), 792 MPa (>10%), 771 MPa (>15%)	Non-linear, Hypoelastic	Truss Element (T3D2)
Sacrotuberous Ligament	326 MPa (5%), 848 MPa (>10%), 826 MPa (>15%)	Non-linear, Hypoelastic	Truss Element (T3D2)

Gluteus Maximus	k = 344 N/mm		Connector Element
Gluteus Medius	k = 779 N/mm		Connector Element
Gluteus Minimus	k = 660 N/mm		Connector Element
Psoas Major	k = 100 N/mm		Connector Element
Adductor Magnus	k = 257 N/mm		Connector Element
Adductor Longus	k = 134 N/mm		Connector Element
Adductor Brevis	k = 499 N/mm		Connector Element

Table 2: Spinopelvic parameters of the finite element models. Low PT refers to anteriorly tilted pelvi, whereas high PT refers to posterior pelvic tilt.

Model	**Sacral Slope (SSº)**	**Pelvic Tilt (PTº)**	**Lumbar Lordosis (LLº)**
PI 36º Low PT	26.7	9.5	41
PI 36º High PT	16.7	19.5	41
PI 41º Low PT	31.7	9.8	46
PI 41º High PT	21.7	19.8	46
PI 46º Low PT	36.7	10	51
PI 46º High PT	26.7	20	51
PI 52º Low PT	41.7	10.4	56
PI 52º High PT	31.7	20.4	56

Supplementary Data

Table 3: Hip validation for peak and average contact stresses [39].

	Joukar et al				Current FE Model			
	Average Contact stress (Mpa)		**Peak Contact stress (Mpa)**		**Average Contact stress (Mpa)**		**Peak Contact stress (Mpa)**	
Motion	**Right**	**Left**	**Right**	**Left**	**Right**	**Left**	**Right**	**Left**
Standing	1.81	1.87	6.2	5.96	1.77	1.875	6.253	5.983
Flexion	1.65	2.29	5.28	5.48	1.97	2.15	6.829	6.946
Extension	1.86	1.76	7.4	5.3	1.78	1.77	5.686	5.268
RB	1.94	1.62	7.1	4.8	1.91	1.81	6.783	5.582
RR	1.66	1.94	6.1	6	1.79	1.93	6.126	6.131

Table 4: Hip validation results for contact area [39].

	Joukar et al		Current FE Model	
	Average Contact area (mm2)		**Average Contact area (mm2)**	
Motion	**Right**	**Left**	**Right**	**Left**
Standing	224	207	218.977	224.105
Flexion	232	222	216.146	258.874
Extension	239	213	208.619	207.565
RB	238	201	214.363	217.741
RR	224	207	217.139	217.586

Table 5: Hip validation for peak contact stresses in various heal-strike scenarios [34, 39, 40].

		Peak Contact Stress					
		Current Study		**Joukar et al.**		**Harris et al.**	**Anderson et al.**
Displacement	**Motion**	**Right Hip**	**Left Hip**	**Right Hip**	**Left Hip**		
R= 10, L=7.5	WHS	18.61	16.41	13.41	10.56	7.52 (5.41 - 9.63)	10.78
R=5, L=4	AHS	17.41	16.21	15.58	13.62	8.53 (5.92 - 11.14)	11.61
R=5, L=4	DHS	17.28	19.23	13.82	13.3	8.66 (5.65 - 11.67)	12.73

Table 6: Hip validation results for average contact stresses in various heal strike scenarios [34, 39, 40].

	Average Contact Stress										
	Current Study				**Joukar et al.**				**Harris et al.**	**Anderson et al**	
	Femur		**Acetabulum**		**Femur**		**Acetabulum**		**FE**	**Experimental**	FE
	Right	**Left**	**Right**	**Left**	**Right**	**Left**	**Right**	**Left**			
WHS	3.52	3.973	3.56	3.35	4.52	4.24	3.73	3.44	1.08 ± 0.32	4.7	5.7
AHS	5.412	4.42	5.13	4.0958	4.73	5.77	3.71	4.48	1.18 ± 0.27	5	5.1
DHS	4.27	4.43	4.08	4.29	4.04	4.82	3.53	4.04	1.23 ± 0.32	4.4	6.2

Table 7: Hip validation results for average hip contact area in various heal strike scenarios [34, 39, 40].

	Contact Area						
	Original FE Model		**Joukar et al**		**Anderson et al.**		**Harris et al.**
	Right Hip	**Left Hip**	**Right Hip**	**Left Hip**	**Experimental**	**FE**	**FE**
WHS	608	603	552	514	425.1	304.2	700 ± 150
AHS	851	848	544	395	321.9	366.1	690 ± 240
DHS	827	800	682	546	375	325	730 ± 160

References

1. Loder, R.T. and E.N. Skopelja, *The epidemiology and demographics of slipped capital femoral epiphysis.* ISRN Orthop, 2011. **2011**: p. 486512.
2. Balch Samora, J., et al., *MRI in idiopathic, stable, slipped capital femoral epiphysis: evaluation of contralateral pre-slip.* J Child Orthop, 2018. **12**(5): p. 454-460.
3. Novais, E.N. and M.B. Millis, *Slipped capital femoral epiphysis: prevalence, pathogenesis, and natural history.* Clin Orthop Relat Res, 2012. **470**(12): p. 3432-8.
4. Lehmann, C.L., et al., *The epidemiology of slipped capital femoral epiphysis: an update.* J Pediatr Orthop, 2006. **26**(3): p. 286-90.
5. Haider, S., D.A. Podeszwa, and W.Z. Morris, *The Etiology and Management of Slipped Capital Femoral Epiphysis: Current Concept Review.* Journal of the Pediatric Orthopaedic Society of North America, 2022. **4**(4).
6. Zupanc, O., et al., *Shear Stress in Epiphyseal Growth Plate is a Risk Factor for Slipped Capital Femoral Epiphysis.* Journal of Pediatric Orthopaedics, 2008. **28**(4): p. 444-451.
7. Gebhart, J.J., et al., *Pelvic Incidence and Acetabular Version in Slipped Capital Femoral Epiphysis.* J Pediatr Orthop, 2015. **35**(6): p. 565-70.
8. Wako, M., et al., *The characteristics of the whole pelvic morphology in slipped capital femoral epiphysis: A retrospective observational study.* Medicine (Baltimore), 2020. **99**(14): p. e19600.
9. Schwab, F., et al., *Gravity line analysis in adult volunteers: age-related correlation with spinal parameters, pelvic parameters, and foot position.* Spine (Phila Pa 1976), 2006. **31**(25): p. E959-67.
10. Roussouly, P., et al., *The vertical projection of the sum of the ground reactive forces of a standing patient is not the same as the C7 plumb line: a radiographic study of the sagittal alignment of 153 asymptomatic volunteers.* Spine (Phila Pa 1976), 2006. **31**(11): p. E320-5.
11. Ghobrial, G.M., Al-Saiegh, F., & Heller, J., *Procedure 31 - Spinopelvic Balance: Preoperative Planning and Calculation*, in *Operative Techniques: Spine Surgery*. 2018, Elsevier. p. 281-287.
12. Legaye, J., et al., *Pelvic incidence: a fundamental pelvic parameter for three-dimensional regulation of spinal sagittal curves.* Eur Spine J, 1998. **7**(2): p. 99-103.
13. Le Huec, J.C., et al., *Pelvic parameters: origin and significance.* Eur Spine J, 2011. **20**

Suppl 5(Suppl 5): p. 564-71.
14. Polly, D.W., et al., *Chapter 31 - Pediatric and Adult Scoliosis*, in *Principles of Neurological Surgery (Third Edition)*, R.G. Ellenbogen, S.I. Abdulrauf, and L.N. Sekhar, Editors. 2012, W.B. Saunders: Philadelphia. p. 497-507.
15. Lazennec, J.Y., A. Brusson, and M.A. Rousseau, *Hip-spine relations and sagittal balance clinical consequences.* Eur Spine J, 2011. **20 Suppl 5**(Suppl 5): p. 686-98.
16. Lazennec, J.Y., et al., *Hip spine relationships: application to total hip arthroplasty.* Hip Int, 2007. **17 Suppl 5**: p. S91-104.
17. Fishkin, Z., et al., *Proximal femoral physis shear in slipped capital femoral epiphysis--a finite element study.* J Pediatr Orthop, 2006. **26**(3): p. 291-4.
18. Shah, H.H., *A finite element study of slipped capital femoral epiphysis (SCFE)*. 2005, State University of New York at Buffalo: United States -- New York. p. 70.
19. Rhyu, K.H., et al., *Application of finite element analysis in pre-operative planning for deformity correction of abnormal hip joints – a case series.* Proceedings of the Institution of Mechanical Engineers, Part H: Journal of Engineering in Medicine, 2011. **225**(9): p. 929-936.
20. Castro-Abril, H.A., F. Galván, and D.A. Garzón-Alvarado, *Geometrical and mechanical factors that influence slipped capital femoral epiphysis: a finite element study.* J Pediatr Orthop B, 2015. **24**(5): p. 418-24.
21. Paseta, O., et al., *Parametric Geometrical Subject-specific Finite Element Models of the Proximal Femur: A Tool to Predict Slipped Capital Femoral Epiphyses.* International Journal of Computational Vision and Biomechanics, 2019. **5**.
22. P. Cignoni, M.C., M. Corsini, M. Dellepiane, F. Ganovelli, G. Ranzuglia, *MeshLab: an Open-Source Mesh Processing Tool.* Sixth Eurographics Italian Chapter Conference, 2008: p. 129-136.
23. Panjabi, M.M., et al., *Mechanical behavior of the human lumbar and lumbosacral spine as shown by three-dimensional load-displacement curves.* J Bone Joint Surg Am, 1994. **76**(3): p. 413-24.
24. Jones, A., *Biomechanical and Finite Element Analyses of Alternative Cements for use in Vertebral*, in *Department of Bioengineering*. 2013, University of Toledo: University of Toledo. p. 125.
25. Palepu, V., *A Thesis entitled Biomechanical Effects of Initial Occupant Seated Posture During Rear End Impact Injury*, in *Department of Bioengineering*. 2013, University of Toledo.

26. Seyed Vosoughi, A., et al., *Optimal satellite rod constructs to mitigate rod failure following pedicle subtraction osteotomy (PSO): a finite element study.* Spine J, 2019. **19**(5): p. 931-941.
27. Kumaran, Y., et al., *Iatrogenic muscle damage in transforaminal lumbar interbody fusion and adjacent segment degeneration: a comparative finite element analysis of open and minimally invasive surgeries.* Eur Spine J, 2021. **30**(9): p. 2622-2630.
28. Ivanov, A.A., et al., *Lumbar fusion leads to increases in angular motion and stress across sacroiliac joint: a finite element study.* Spine (Phila Pa 1976), 2009. **34**(5): p. E162-9.
29. Lindsey, D.P., et al., *Sacroiliac Joint Fusion Minimally Affects Adjacent Lumbar Segment Motion: A Finite Element Study.* Int J Spine Surg, 2015. **9**: p. 64.
30. Gerber, J., *Biomechanical Evaluation of Facet Bone Dowels in the Lumbar Spine*, in *Department of Bioengineering*. 2015, University of Toledo: University of Toledo. p. 128.
31. Wu, G., et al., *ISB recommendation on definitions of joint coordinate system of various joints for the reporting of human joint motion--part I: ankle, hip, and spine. International Society of Biomechanics.* J Biomech, 2002. **35**(4): p. 543-8.
32. Mechlenburg, I., et al., *Cartilage thickness in the hip joint measured by MRI and stereology--a methodological study.* Osteoarthritis Cartilage, 2007. **15**(4): p. 366-71.
33. Rachakonda, P., *Sphere Fit*. 2023, MATLAB Central File Exchange: MATLAB Central File Exchange.
34. Anderson, A.E., et al., *Validation of finite element predictions of cartilage contact pressure in the human hip joint.* J Biomech Eng, 2008. **130**(5): p. 051008.
35. Goker, B., et al., *The radiographic joint space width in clinically normal hips: effects of age, gender and physical parameters.* Osteoarthritis Cartilage, 2003. **11**(5): p. 328-34.
36. Stewart, K.J., et al., *Implementing capsule representation in a total hip dislocation finite element model.* Iowa Orthop J, 2004. **24**: p. 1-8.
37. Phillips, A.T., et al., *Finite element modelling of the pelvis: inclusion of muscular and ligamentous boundary conditions.* Med Eng Phys, 2007. **29**(7): p. 739-48.
38. Bergmann, G., et al., *Hip contact forces and gait patterns from routine activities.* J Biomech, 2001. **34**(7): p. 859-71.
39. Joukar, A., et al., *Effects on hip stress following sacroiliac joint fixation: A finite element study.* JOR Spine, 2019. **2**(4): p. e1067.
40. Harris, M.D., et al., *Finite element prediction of cartilage contact stresses in normal human hips.* J Orthop Res, 2012. **30**(7): p. 1133-9.
41. Yadav, P., S.J. Shefelbine, and E.M. Gutierrez-Farewik, *Effect of growth plate geometry*

and growth direction on prediction of proximal femoral morphology. J Biomech, 2016. **49**(9): p. 1613-1619.
42. Farzaneh, S., O. Paseta, and M.J. Gomez-Benito, *Multi-scale finite element model of growth plate damage during the development of slipped capital femoral epiphysis.* Biomech Model Mechanobiol, 2015. **14**(2): p. 371-85.
43. Kumaran, Y., et al., *Effects of Sacral Slope Changes on the Intervertebral Disc and Hip Joint: A Finite Element Analysis.* World Neurosurg, 2023. **176**: p. e32-e39.
44. Gebhart, J.J., et al., *Relationship between pelvic incidence and osteoarthritis of the hip.* Bone & Joint Research, 2016. **5**(2): p. 66-72.
45. Bao, H., et al., *Lumbosacral stress and age may contribute to increased pelvic incidence: an analysis of 1625 adults.* Eur Spine J, 2018. **27**(2): p. 482-488.
46. Negrini, S., et al., *Sagittal Balance in Children: Reference Values of the Sacral Slope for the Roussouly Classification and of the Pelvic Incidence for a New, Age-Specific Classification.* Applied Sciences-Basel, 2022. **12**(8).
47. Sankar, W.N., et al., *Acetabular morphology in slipped capital femoral epiphysis.* J Pediatr Orthop, 2011. **31**(3): p. 254-8.
48. Bauer, J.P., D.R. Roy, and S.S. Thomas, *Acetabular retroversion in post slipped capital femoral epiphysis deformity.* J Child Orthop, 2013. **7**(2): p. 91-4.
49. Monazzam, S., et al., *Is the Acetabulum Retroverted in Slipped Capital Femoral Epiphysis?* Clinical Orthopaedics and Related Research®, 2013. **471**(7): p. 2145-2150.
50. Siebenrock, K.A., D.F. Kalbermatten, and R. Ganz, *Effect of Pelvic Tilt on Acetabular Retroversion: A Study of Pelves From Cadavers.* Clinical Orthopaedics and Related Research®, 2003. **407**: p. 241-248.
51. Henak, C.R., et al., *Patient-specific analysis of cartilage and labrum mechanics in human hips with acetabular dysplasia.* Osteoarthritis Cartilage, 2014. **22**(2): p. 210-7.
52. Song, S.K., et al., *Changes of acetabular anteversion according to pelvic tilt on sagittal plane under various acetabular inclinations.* Journal of Orthopaedic Research, 2021. **39**(4): p. 806-812.
53. Hesper, T., et al., *Acetabular Retroversion, but Not Increased Acetabular Depth or Coverage, in Slipped Capital Femoral Epiphysis: A Matched-Cohort Study.* JBJS, 2017. **99**(12): p. 1022-1029.
54. Yoshimoto, H., et al., *Spinopelvic Alignment in Patients With Osteoarthrosis of the Hip: A Radiographic Comparison to Patients with Low Back Pain.* Spine, 2005. **30**(14): p. 1650-1657.

55. Maurer, E., et al., *Lack of correlation between hip osteoarthritis and anatomical spinopelvic parameters obtained in supine position on MRI.* Injury, 2023. **54**(2): p. 525-532.
56. Wiemann, J.M.I. and J.A. Herrera-Soto, *Can We Alter the Natural History of Osteoarthritis After SCFE With Early Realignment?* Journal of Pediatric Orthopaedics, 2013. **33**: p. S83-S87.
57. Abraham, E., et al., *Clinical Implications of Anatomical Wear Characteristics in Slipped Capital Femoral Epiphysis and Primary Osteoarthritis.* Journal of Pediatric Orthopaedics, 2007. **27**(7): p. 788-795.
58. Helgesson, L., et al., *Early osteoarthritis after slipped capital femoral epiphysis.* Acta Orthop, 2018. **89**(2): p. 222-228.
59. de Poorter, J.J., et al., *Long-term outcomes of slipped capital femoral epiphysis treated with in situ pinning.* Journal of Children's Orthopaedics, 2016. **10**(5): p. 371-379.
60. Brand, R.A., *Joint contact stress: a reasonable surrogate for biological processes?* Iowa Orthop J, 2005. **25**: p. 82-94.
61. Chen, H.-F. and C.-Q. Zhao, *Pelvic incidence variation among individuals: functional influence versus genetic determinism.* Journal of Orthopaedic Surgery and Research, 2018. **13**(1): p. 59.
62. Joukar, A., et al., *Sex Specific Sacroiliac Joint Biomechanics During Standing Upright: A Finite Element Study.* Spine (Phila Pa 1976), 2018. **43**(18): p. E1053-E1060.
63. Goel, V.K., et al., *Effects of charite artificial disc on the implanted and adjacent spinal segments mechanics using a hybrid testing protocol.* Spine (Phila Pa 1976), 2005. **30**(24): p. 2755-64.
64. Dalstra, M., R. Huiskes, and L. van Erning, *Development and validation of a three-dimensional finite element model of the pelvic bone.* J Biomech Eng, 1995. **117**(3): p. 272-8.
65. Butler, D.L., et al., *Location-dependent variations in the material properties of the anterior cruciate ligament.* J Biomech, 1992. **25**(5): p. 511-8.